USGS
science for a changing world

U.S. DEPARTMENT OF THE INTERIOR
U.S. GEOLOGICAL SURVEY

PRELIMINARY SCIENTIFIC RESULTS OF THE CREEDE CALDERA CONTINENTAL SCIENTIFIC DRILLING PROGRAM

P.M. Bethke, Editor

Open-File Report 94-260-I

2001

SULFUR, CARBON AND OXYGEN SYSTEMATICS DURING DIAGENESIS AND FLUID INFILTRATION IN THE CREEDE CALDERA, COLORADO

By

Robert P. Ilchik[1]
Douglas Rumble III
Carnegie Institution Of Washington
Geophysical Laboratory
Washington, DC

[1] Present address:
645 W. Orange Grove Rd., Apt 1038
Tucson, AZ 85704

CHAPTER I

SULFUR, CARBON AND OXYGEN SYSTEMATICS DURING DIAGENESIS AND FLUID INFILTRATION IN THE CREEDE CALDERA, COLORADO

Robert P. Ilchik
Douglas Rumble, III
Carnegie Institution of Washington
Geophysical Laboratory
5251 Broad Branch Road
Washington, DC 20015-1305

ABSTRACT

Sulfides and attendant vein minerals present in drill core recovered during the Creede Moat Drilling Project were examined to determine distribution and isotopic compositions. Sulfides are present in three lithologically distinct units in hole CCM-2. These are, from top to bottom: 1) Creede Formation lacustrine turbidites; 2) volcanic megabreccia; and, 3) Snowshoe Mountain ash-flow tuff. In the Creede Formation pyrite is commonly present at the top and/or base of turbidites, but is has only a minor presence in varves. Pyrite is also present as stalactites in travertine bodies found along the paleo-shoreline. Pyrite, without calcite, is found over a vertical span of 52 meters (170 feet) in older fractures and replacing magnetite in the upper portions of the volcanic megabreccia. Fresh magnetite is present in similar underlying host rocks. In the ash-flow and the base of the megabreccia, pyrite occurs in veins with calcite and as replacements of magnetite and biotite near veins. Framboidal pyrite is common to abundant in these veins, suggesting bacterial processes may have been involved in its formation. Samples from two environments, one in the Creede Formation and the other in the ash-flow, have $\delta^{34}S$ variations of nearly 100‰. In addition, vein calcites from the ash-flow have a large variation and display a distinct, inverse correlation.

The data have been used to develop a model for sulfur input into Lake Creede. We suggest that most of the sulfur was input directly into the lake as volcanic H_2S during residual degassing following eruption of the caldera and during subsequent dome building. The presence of an unsulfidized zone in the megabreccia indicates that neither ascending nor descending, H_2S-bearing fluids completely penetrated this unit. Thus, pyrite occurrences above and below this barrier must be viewed as being hydrologically separate. This

separation further suggests that the veins in the ash-flow formed prior the deposition of most of the megabreccia. Fumaroles transporting H_2S deposited near 0‰ pyrite in the ash-flow during ascent through this unit. H_2S which vented to the surface collected in small ponds, where it was available for bacterial oxidation and reduction reaction. During deposition of the Creede Formation, fumarolic H_2S released into the water column reacted with sedimentary iron to form pyrite during and shortly after turbidite flows. Bacterial reduction probably played only a minor role in pyrite formation as evidenced by the paucity of framboids and organic matter in the Creede Formation.

INTRODUCTION

The purpose of this investigation was to document the various occurrences and isotopic compositions of sulfides and associated minerals encountered in the Creede Moat Drilling Project. The project consisted of drilling two core holes (CCM-1 and CCM-2) into the lacustrine sediments of the Creede Formation and into the underlying volcanic rocks (Bethke, et al, Chapter A, this volume). Selected samples from drill hole CCM-2 have been examined to determine mineralogical, elemental and isotopic compositions. Mineralogical and elemental data for volcanic and sedimentary sequences were used as a guide to isotopic investigations

The rocks in hole CCM-2 can be divided into three major lithologic units. The uppermost unit which extends from the collar to a depth of approximately 475 meters (1558 feet) is called the Creede Formation in this report. The Creede Formation consists primarily of a varve facies and various turbidite facies. The varve facies is composed of alternating laminations of carbonate and siliciclastic material with each cycle averaging about 500 μm in thickness. Turbidite facies consist of both proximal turbidites which grade from medium or coarse sands to silt or clay, and distal turbidites that consist exclusively of silt and/or clay. Between 475 meters and approximately 654 meters (2145 feet) the section consists of a heterolithic volcanic megabreccia with minor lacustrine sandstones. From 654 meters to the end of hole at 706.8 meters (2319 feet) is a sanidine, biotite ash-flow tuff referred to as the Snowshoe Mountain Tuff. More extensive descriptions of these rock units can be found elsewhere in this report, but a careful reader should note that there is a difference between where the top of the Snowshoe Mountain tuff is placed in this chapter and where others have placed this contact (i.e., Larsen and Crossey, Chapter E, this volume). Sulfur isotopic measurements were made on pyrite from the three major rock units in hole CCM-2, and cover a variety of habits and occurrences. Carbon and oxygen

isotopic measurements were made on vein calcite which accompanies pyrite in the basal tuff unit, and from calcite veins in the megabreccia and Creede Formation which do not contain sulfides. This report will present our preliminary findings.

METHODS

All analyses have been carried out utilizing facilities at the Geophysical Laboratory. Mineralogical and compositional determinations were made using optical microscopy or a JEOL Superprobe electron microprobe. Determinations of carbon and oxygen isotopic variations in carbonates were made utilizing phosphoric acid dissolution (McCrea, 1950). Sulfur isotopic variations were determined using the SF_6 method of Puchelt et al. (1971); combined with an infrared laser for spot heating of the sample (Rumble et al., 1993). This method allows for the resolution of isotopic zoning on the scale of 100 μm, and has a reproducibility on standards of better than 0.2‰. Isotopic data are reported in per mil variation from standards using the delta notation (c.f., Ohmoto and Rye, 1979). Standards for reporting purposes are Pee Dee Belemite for carbon; V-SMOW for oxygen; and Canyon Diablo troilite for sulfur.

RESULTS

Pyrite is by far the major sulfide present in hole CCM-2, but small amounts of sphalerite and possibly chalcopyrite are also present. Pyrite is present in all major stratigraphic units in the hole, but occurrence and morphology vary greatly depending upon the host rock. Sulfur isotopic compositions are summarized in Figure 1. Stratigraphic variations in pyrite occurrences and $\delta^{34}S$ are presented below.

Snowshoe Mountain Tuff

Within the Snowshoe Mountain Tuff, pyrite is dominantly found in veins, with local dissemination extending up to ~ 1 cm into the host rock. Pyrite is generally the only sulfide present. Sphalerite, as euhedral grains up to 30 μm in diameter, was found in a few veins (most notably sample 2R223-8.5), and a minute amount of what appears to be chalcopyrite was also present with sphalerite in sample 2R223-8.5. Three morphologies of vein pyrite are common: 1) framboids from 20 to 40 μm in diameter composed of aggregates of pyritohedra ~ 1 μm in diameter; 2) euhedral, coffin-shaped crystals up to 150 μm in length which often grow radially from framboids: and, 3) fine irregular breccia fragments up to 100 μm in diameter. Accumulations of any or all three types form masses from < 100 μm up to 3 mm thick on the

footwall side of the vein. The hanging wall is rarely more than 100 to 200 μm thick. Veins are usually filled and closed by a later calcite.

Disseminated pyrite is common within the immediate vicinity of veins. It is found either with biotite or a titanium oxide and apatite. The latter association indicates the replacement of magnetite, which elsewhere in the tuff is associated with apatite microphenocrysts, and contains minor amounts of titanium.

Vein pyrite, sphalerite and calcite in the tuff show little chemical variation based on electron microprobe analyses. Pyrite does not contain any elements other than iron and sulfur at levels of detection (~ 0.5 wt. %). Sphalerite appears to be weakly zoned with regard to iron. The cores of grains contain approximately 2.0 wt. per cent iron, whereas a 5 μm thick rim contains roughly 3.5 wt. per cent iron. The chalcopyrite grain was too a small to obtain an accurate analysis using the electron microprobe. Calcite contains a variable, but limited amount of MgO (< ~ 1-2%).

Stable isotopic compositions for vein minerals show remarkable variations from -17‰ to +80‰ relative to C.D.T. Similar variations, determined by SHRIMP microprobe analysis, are reported by McKibben and Eldridge (Chapter H, this volume). (Almost this entire range is seen in one vein (2R224-1.2) but the extreme ^{34}S enrichment was found in an adjacent specimen as well (2R225-0.55). Most veins, however, show a variation of less than 10‰ (Fig. 2). $\delta^{34}S$ values have a strong maxima near 0‰, with a much smaller mode near 40‰ (Fig. 3).

Specimen 2R224-1.2 is from a depth of 671.2 meters (2202 feet), 17.4 meters below the contact with the megabreccia. The vein is 5.5 mm thick and is nearly flat lying. Pyrite on the hanging wall is 500 μm thick; the footwall is 3 mm. The rest of the vein is filled with calcite. The lower two-thirds of the footwall is composed of euhedral pyrite grains up to 500 μm in diameter, most of which are cored by a ~ 30 μm framboid. This is capped by a band of laminated pyrite about 200 μm thick, which in turn is overlain by an accumulation of framboids up to 2 mm thick. The lower sequence shows a nearly constant $\delta^{34}S$ of -11 to -8‰ (4 samples); the banded layer is +17‰ (1 sample), and the framboid layer is +66‰ (1 sample). A similar pattern is present in the hanging wall, but the heaviest value measured was + 37‰. Specimens 2R225-0.55 and 2R225-4.4 are less than 1.5 meters away. Both contain framboids, and are also enriched in ^{34}S. Pyrite in the other veins sampled was generally an accumulation of brecciated fragments and consisted of only scattered framboids.

Vein calcites have a relatively large isotopic range and show an unusual inverse covariance between $\delta^{13}C$ and $\delta^{18}O$. $\delta^{13}C$ varies from -6‰ to -16‰ relative to P.D.B., whereas $\delta^{18}O$ varies +4‰ to +22‰ relative to SMOW (Fig. 4). Although a few samples have intermediate values, most analyses are

clustered near one extreme or the other. Calcite found along the margins in contact with pyrite is generally botryoidal in habit with a green clay separating layers up to 1 mm thick. This calcite tends to be more enriched in ^{18}O and depleted in ^{13}C. Most of the samples enriched in ^{13}C are a coarse, white calcite and come from the central positions of the veins. Thus, it appears that calcite isotopic compositions change with time towards heavier carbon and lighter oxygen.

Volcanic megabreccia

Pyrite is the only sulfide identified in the megabreccia and its occurrence is restricted to the upper 52 meters, and the lowest meter or so of the unit. Elsewhere magnetite is common in the megabreccia. In the upper portion of the megabreccia, pyrite occurs along fractures as individual euhedral crystals or as thin (< 200 μm) selvages. It is also found as 10 to 20 μm octahedra disseminated in the volcanic fragments, pearlitic glass and sanidine phenocrysts. Some disseminated pyrite is similar to that seen in the ash-flow unit in that it is associated with a titanium oxide and apatite, or more rarely with biotite. A small amount of quartz is present in some lithophysal cavities associated with pyrite and glass altered to pearlite. Pyrite in the megabreccia differs morphologically from the underlying veins in that it is dispersed as individual grains on the fractures, rather than as continuous masses, and that little or no carbonate is present with the pyrite. Elemental data are not yet available.

At the base of the unit (specimen 2R218-2.5), vein pyrite is found in association with quartz. These veins have been re-brecciated, and are present as small clasts found with other rock fragments. Pyrite framboids are also present in this sample, but they have not been seen in specimens from the upper pyrite zone.

Pyrite $\delta^{34}S$ values range from + 4‰ to + 33‰ in the upper portion of the megabreccia, with most samples yielding values greater than + 20‰. A single sample of brecciated pyrite with quartz from near the base of the unit has a $\delta^{34}S$ of + 43.2‰. This value is almost identical to vein pyrite at the top of the underlying ash-flow.

Throughout the megabreccia, a set of non-pyrite bearing fractures is present. Calcite fills much of the void space produced by this later brecciation. This calcite is white, coarsely crystalline or skeloidal (e.g., 2R216-8.9) and has a satiny luster. It is similar in appearance and isotopic composition to late calcite found in the ash-flow. The veins are generally less than a few mm wide. In spite of an intensive search, no veins were found in breccia fragments that clearly did not cut the breccia matrix as well. Several veins appeared to not cut matrix in hand specimen, but upon close inspection, calcite was found in the matrix (e.g., 2R201-6.55). Thus it can be concluded

that the calcite veins formed after brecciation. $\delta^{13}C$ and $\delta^{18}O$ from calcite varied from - 5.4‰ to - 6.7‰ PDB, and + 3.5 to + 10.3‰ SMOW, respectively (Fig. 5). These values are similar to the group of heavy-carbon, light-oxygen calcites in the ash-flow. However, these samples show a positive correlation between the two isotopes, with a slope of 0.5.

Sedimentary Rocks

Pyrite is widely distributed vertically in the sedimentary sequence, but is dominantly associated with turbidites. Within a turbidite, pyrite is present near both the base and the top of individual sequences (. 6). Pyrite in basal sandstone layers appears to be an intergranular cement. Near the tops of beds it is found as disseminated octahedral grains about 10 μm in size, and in some cases, its abundance increases towards the top of the bed (e.g., 2R130-1.0). Pyrite is rare to non existent within varve sequences.

Calcite is present primarily as one component of the varve couplet and as a minor component of turbidites. A limited number of calcite veins are also present in the Creede Formation, but these veins lack pyrite.

$\delta^{34}S$ values for lacustrine samples range from - 13‰ to + 23‰. The results are relatively evenly distributed across the range of values. Similar results have been found from other portions of the unit (Rye, et al., Chapter G, this volume) The low end of the range is similar to that seen in the tuff, but enrichments in ^{34}S are not as extreme as in the deeper veins. Descriptions of two samples analyzed in detail are given below.

Specimen 2R106-1.4 (Fig. 7) contains of 5 bands of pyrite up to 700 μm thick. The middle three bands are continuous, whereas the upper and lower bands are not. Each band straddles the contact between coarse- to medium-grained turbidite sandstones. The bands are nearly evenly spaced over an interval of 10 to 12 mm. One pyrite band is cut by a small thrust fault, which contains analcime in its nappe. This and the lack of fine-grained sediment in the sample indicate that pyrite deposition was early and proceeded most diagenesis. Pyrite is also present as irregular "flames" and "sags" between the middle three bands. Multiple analyses of each band reveal a zonation in $\delta^{34}S$ of +15‰ to +20‰ across each of the major bands. The bases of the lower two main bands are near +15‰, whereas the tops are near 0‰. For the upper band the pattern is reversed: the base is near +5‰, and the top is nearly +25 ‰. Pyrite between the bands has an isotopic composition that varies only slightly from +15.7‰ to +19.3‰.

Specimen 2R130-1.0 consists of several turbidites alternating with varve sequences. One complete turbidite which grades from medium-grained sand to fine silt is present. The other clastic units are silt and clay sized. These probably represent distal turbidites. Microprobe data show that pyrite is strongly associated with portions of the turbidites, but that the varves are

nearly devoid of sulfur (Fig. 6). Iron is present throughout the specimen regardless of the sulfur content. The highest concentration of pyrite (over 50 wt. %) is present over an interval of 1 to 2 mm at the base of the complete turbidite. This pyrite appears to be an intergranular cement. Pyrite is also present in the finer-grained portions of this turbidite, and reaches concentrations of greater than 15 wt. per cent over an interval of 1 mm at the top of the bed. Slightly higher in the specimen, pyrite is present in concentrations of up to about 10 wt per cent in fine-grained turbidites. $\delta^{34}S$ from the near massive zone at the base of the complete turbidite varies from -13.5‰ to -12.2‰. Within the mid-portions of this bed, $\delta^{34}S$ in three analyses was nearly constant from -5.0‰ to -4.1‰. At the top of the bed $\delta^{34}S$ is +2.2‰. In the three closely associated, finer-grained beds near the top of the specimen $\delta^{34}S$ varies from ~ 0‰ in the lowest bed to -8.1‰ in the upper bed. The isotopic composition within the upper bed appears to also be nearly constant.

Pyrite has also been found at outcrops of Creede Formation above the dill hole collars. Pyrite is found in fractures below a travertine body at the Silver Horde at the Monon Hill mine about 2 km NNW, and about 115 meters above the collar elevation of CCM-2. (sample PMB-AAM-1003, courtesy of P.M. Bethke). There it is found as stalactites and other dripstone habits, which grow up to 3.5 mm in diameter. One sample was analyzed in detail. This sample has a variation in $\delta^{34}S$ of 90‰, from -17.7‰ at the core to + 73.3‰ at the rim. Interestingly, these values are almost identical to those found in the ash-flow.

$\delta^{13}C$ and $\delta^{18}O$ for 2 samples of vein calcite are -5.1‰ and -0.1‰ PDB, and +5.6‰ and +5.5‰ SMOW, respectively. These data are also in agreement with analyses of other veins by Rye and others.

DISCUSSION

No single process seems to explain the isotopic fractionation trends found to date in specimens from CCM-2. The variety of processes range from simple mixing of two reservoirs, Rayleigh fractionation during reduction of SO_4^{2-} to H_2S, probably by bacterial means, and precipitation from reactions of H_2S with labile iron in the various lithologies. Some pyrite formed from H_2S-bearing solutions which advected through fractures in the volcanic units, or along permeable horizons in the Creede Formation. Whereas, it appears that pyrite was also formed when H_2S-bearing fluids interacted with sediments while in suspension and/or during compaction and dewatering.

Mixing appears to have been important in the formation of the stalactite from the Monon Hill mine. The near straight line connecting centers of mass for individual sample points collected in this specimen suggests mixing

between a depleted reservoir with $\delta^{34}S$ of -20‰ and an enriched reservoir with a $\delta^{34}S$ of +80‰ (Fig. 8). A Rayleigh fractionation event can not be fit to these data because of the straight-line relationships seen when the data are portrayed in a manner consistent with the concentric symmetry of the specimen. Although mixing accounts for the fractionations seem in the sample, it does not shed light on the more fundamental question of how and where did these separate reservoirs develop -- especially the enriched one.

Within the Creede Formation there is only minor evidence for sulfate reduction by bacteria. The limited amount of preserved organic matter (Leventhal, Chapter K, this volume, 1995; Reynolds and Rosenbaum, Chapter M, this volume) and paucity of framboidal pyrite do not support the suggestion of large-scale bacterial sulfate reduction. Furthermore, many of the isotopic patterns in the samples are in conflict with large, negative fractionations factors between the sulfur reservoir and pyrite as would be the case in sulfate reduction. Indeed, many specimens show decreasing $\delta^{34}S$ trends with time (e.g., the lower bands in 2R106-1.4, and the upper bands in 2R130-1.0), indicative of pyrite deposition directly from H_2S-bearing fluids. Advection of an H_2S-bearing fluid may have played a role in the formation of pyrite in some of the sandstones where it appears to be a cement. Precipitation of pyrite directly from fluid that has migrated and reacted over some distance could account for the low $\delta^{34}S$ values found in the sandstone portion of specimen 2R130-1.0.

Evidence for limited bacterial activity to fix sulfur as pyrite is found in the framboid-bearing veins in the ash-flow tuff and the base of the megabreccia. The isotopic data fit relatively well with a Rayleigh fractionation model for the reduction of SO_4^{2-} (Fig. 9), considering the uncertainties in the mass fraction of each band, and whether or not the entire sequence is present. bacteriogenic fractionation of sulfur isotopes during sulfate reduction is a kinetic process dependent largely upon the nutrient supply to the bacteria (Kemp and Thode, 1968). Under conditions when nutrients are abundant and do not limit growth rates, only minimal isotopic fractionation has been observed. However, when nutrients are limited, observed kinetic fractionations approaches the equilibrium fractionation between sulfate and sulfide at the temperature of interest. The scarcity of preserved organic matter indicates that the nutrient supply was limited during history of the lake occupying the Creede caldera moat. If this were the case, then fractionation should be close to the equilibrium value, and may indicate the temperature under which the process took place. Using various mass distributions for specimen 2R224-1.2, Rayleigh models indicate that reduction took place at temperatures between about 40°C and 100°C.

For the most part, however, it appears that vein pyrite in the ash-flow precipitated directly from an H_2S-bearing fluid. Evidence for this is the

major mode in isotopic values at -5‰ to 0‰ found in the deep veins and the lack of fractionation between early and late pyrite in most veins. This is also supported by the scarcity of framboids and other direct evidence for microbial sulfate reduction in most veins.

MODEL FOR DEVELOPMENT OF LAKE CREEDE

A reasonable means to achieve the elemental and isotopic patterns found in CCM-2 that is consistent with the geologic setting is to have the vast majority of the sulfur introduced as H_2S by fumaroles or hydrothermal discharge (Fig 10). If this were the case, then most of the pyrite in the ash-flow formed by direct reaction of Fe-bearing phases with H_2S. Framboids present in the upper portions of the ash-flow and in the base of the megabreccia could be the result of H_2S vented to the surface that then oxidized and accumulated in small ponds or an ephemeral lake (Larsen and Crossey, Chapter E, this volume, 1996). This sulfur was then available for bacterial reduction, which led to the strong ^{34}S enrichments. Framboidal pyrite could have formed at the surface and been transported to shallow depths. Alternatively, this fluid could have percolated back into the tuff a short distance before it was reduced and formed pyrite.

Botryoidal, early calcite (low $\delta^{13}C$, high $\delta^{18}O$) in pyrite veins in the ash-flow tuff could have formed from hypogene fluids that had not yet interacted with the surface. In the case of the early calcite, fluid temperatures of 70°C to 80°C would put these samples in isotopic equilibrium with fluids with an $\delta^{18}O$ near that present in primary fluid inclusions from the OH vein (Bethke and Rye, 1979). Carbon in these samples would be in equilibrium with an aqueous CO_2 with an isotopic composition of -22‰. If this were the case then this indicates that the carbon came from an organic source. Later, sparry calcite could have formed from descending fluids that had collected and evolved in an early lacustrine setting. In this case carbon was derived primarily from the atmosphere and oxygen from meteoric water.

The presence of a magnetite-bearing zone in the lower and mid-parts of the megabreccia indicates that H_2S-bearing fluids did not pass through this unit at the location of the drill hole, regardless of whether the fluid was descending or ascending. It also appears that the veins in the ash-flow and the base of the megabreccia formed prior to the deposition of the majority of the megabreccia. This is supported by the fact that pyrite veins do not extend higher into the megabreccia, suggesting that some erosion took place prior to the deposition of the majority of this unit.

A mechanism for pyrite deposition at the top of the megabreccia is unclear. One possibility is for H_2S-bearing fluids to percolate into the breccia from the lake. This hypothesis is not strongly supported by the isotopic

evidence because the megabreccia is more enriched in ^{34}S than the sediment. Alternatively, the lake sediments could have acted as a seal that trapped hypogene H_2S at the top of the megabreccia beneath the sediments. Again this hypothesis is not well supported by the isotopic data.

After deposition of the megabreccia and the establishment of a lacustrine regimen, fumarolic activity could have triggered turbidites along the margins of the moat (Fig. 11). As these sediments moved down slope and settled out of suspension, iron in the sediment mixed with H_2S from the fumarole and pyrite was precipitated. Support for this mechanism is found in the turbidites of specimen 2R130-1.0. Within individual turbidites, little variation is seem in $\delta^{34}S$, indicating that a single homogenous source for the sulfur. Whereas, between the upper three beds there is a moderate depletion in ^{34}S. The size of this depletion is what would be expected from the deposition of pyrite at a temperature of 20°C or less. The extreme depletion in ^{34}S found in the basal sandstone in specimen 2R130-1.0 could be due to advection of fluid along this relatively porous bed as suggested by the morphology of the pyrite. Alternatively, H_2S could have been discharged into the basin but remained unreacted until turbidites, triggered by some other mechanism, mixed sediment with these fluids and caused pyrite precipitation.

Bacterial processes to produce H_2S from the reduction of SO_4^{2-} do not appear to have been of major importance in the lake. Evidence for this is provided by 1) the low abundance of organic matter preserved in the lake (Leventhal, Chapter K, this volume, 1995); 2) the morphology of the lacustrine pyrite; 3) the association of pyrite with turbidites rather than the more slowly deposited varve units; and 4) the relatively even distribution of isotopic compositions. Furthermore, under the conditions in the lake (i.e., calcite supersaturation, Larsen and Crossey, (Chapter E, this volume, 1996); pH ~7.5, Finkelstein (1997); and CO_2 in equilibrium with the atmosphere) the maximum concentration of SO_4^{2-} in the lake water could be only about 100 ppm. Assuming that the lake is 100 m deep, quantitative precipitation of sulfate from the water column would produce a layer of pyrite approximately 1 mm thick. Although the calculated sulfate concentration is very sensitive to pH (one log unit increase in pH, increases SO_4^{2-} concentration by two log units), the presence of numerous pyrite layers, often deposited in apparent rapid succession would seem to preclude sulfate reduction as a major process in the formation of pyrite.

ONGOING WORK

Additional work needs to be done on pyrite from the Creede Formation. to confirm the limited range of ^{34}S enrichments, and to look for other cases

indicating a depletion in ^{34}S over short time intervals such as that shown by specimen 2R130-1.0. If the hypotheses of hypogene H_2S is accepted, then the Creede Formation contains a chronologically sequenced set of samples of a major portion of the devolatilization history of a post-eruptive caldera.

ACKNOWLEDGMENTS

We would like to express our gratitude to our colleague at the Geophysical Laboratory Tom Hoering whose development of the SF_6 technique made this study possible. The project was supported by NSF grant EAR 9115965. We also want to thank all the other investigators on this project. Their work has greatly contributed to our understanding of the overall history of the lake, but they should not be held accountable for our interpretations.

REFERENCES

Bethke, P. M., and Rye, R. O., 1979, Environment of ore deposition in the Creede mining district, San Juan Mountains, Colorado: Part IV. Source of fluids from oxygen, hydrogen, and carbon isotope studies: Economic Geology v. 74, p 1832-1851.

Finkelstein, D.B., 1997, Origin and diagenesis of lacustrine sediments of the late Oligocene Creede Formation, Southwestern Colorado: unpublished Ph.D. thesis, University of Illinois at Urbana-Champaign, Urbana, Illinois, 144 p.

Kemp, A. L. W., and Thode, H. G., 1968, The mechanism of the bacterial reduction of sulphate and of sulphite from isotope fractionation studies: Geochimica et Cosmochimica Acta, v. 32, p. 71-91.

Larsen, D. and Crossey, L.J., 1996, Depostional environments and paleolimnology of an ancient caldera lake: Oligocene Creede Formation, Colorado: Geological Society of America Bulletin, v. 108, p. 526-544.

Leventhal, J.S. 1995, Carbon-sulfur plots to show diagenetic and epigenetic sulfidation in sediments: Geochimica et Cosmochimica Acta, v. 59, p. 1207-1211.

McCrea, J. M., 1950, On the isotope chemistry of carbonates and paleotemperature scale: Journal of Chemical Physics, v. 18, p. 849-857.

Ohmoto, H., and Rye, R. O., 1979, Isotopes of sulfur and carbon, *in* Barnes, H. L., ed., Geochemistry of Hydrothermal Ore Deposits, 2nd edition: New York, Wiley Interscience, p. 509 - 567.

Puchelt, H., Sabels, B. R., and Hoering, T. C., 1971, Preparation of sulfur hexafluoride for isotope geochemical analysis: Geochimica et Cosmochimica Acta, v. 35. p 652-628.

Rumble, D., Hoering, T. C., and Palin, 1993, Preparation of SF_6 for sulfur isotope analysis by laser heating sulfide minerals in the presence of F_2 gas: Geochimica et Cosmochimica Acta, v. 57, p. 4499-4512.

FIGURE CAPTIONS

Figure 1: Vertical distribution of $\delta^{34}S$ in CCM-2

Figure 2: Depth profiles for veins in the ash-flow tuff.

Figure 3: Histograms of $\delta^{34}S$ results for the major rock units in CCM-2. Out line encloses all analyses; filled areas include average values where multiple analyses were done on the same sample.

Figure 4: $\delta^{13}C$ and $\delta^{18}O$ data for vein calcite in CCM-2.

Figure 5: Depth profile of $\delta^{13}C$ and $\delta^{18}O$ data.

Figure 6: Depth profile for specimen 2R130-1.0. Data for elemental abundances from microprobe scans collected at 10 μm spacing, and averaged over 70 μm. Seven scans were completed perpendicular to bedding to remove local biasing of data.

Figure 7: Depth profile for specimen 2R106-1.4. See text for description.

Figure 8: $\delta^{34}S$ profile across stalactite from the Monon Hill mine. A. Data presented as a function of distance from center of the stalactite. B. Distance axis transformed to account for the concentric symmetry of the stalactite.

Figure 9: Rayleigh fractionation models for sulfate reduction to form pyrite in specimen 2R224-1.2. A. Model assuming closed system behavior during formation of entire vein. B. Model assumes open system during deposition of most of "megacryst" zone (not shown), followed by closed system behavior during last portion of "megacryst" zone and later layers.

Figure 10: Model for early development of moat lake and vein pyrite deposition.

Figure 11: Model for later stages of moat lake and pyrite deposition in lacustrine sediments of the Creede Formation.

Fig 1.

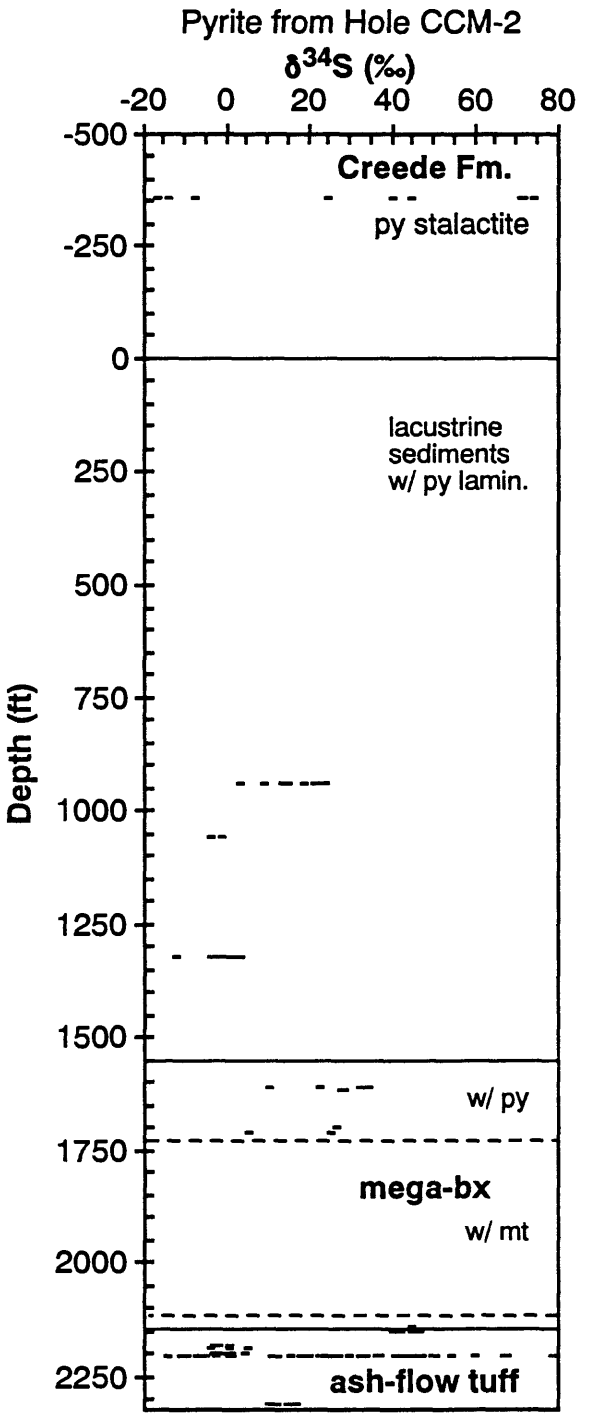
Pyrite from Hole CCM-2
δ34S (‰)
-20
0
20
40
60
80
-500
-250
0
250
500
750
1000
1250
1500
1750
2000
2250
Depth (ft)
Creede Fm.
py stalactite
lacustrine
sediments
w/ py lamin.
w/ py
mega-bx
w/ mt
ash-flow tuff

Fig. 2

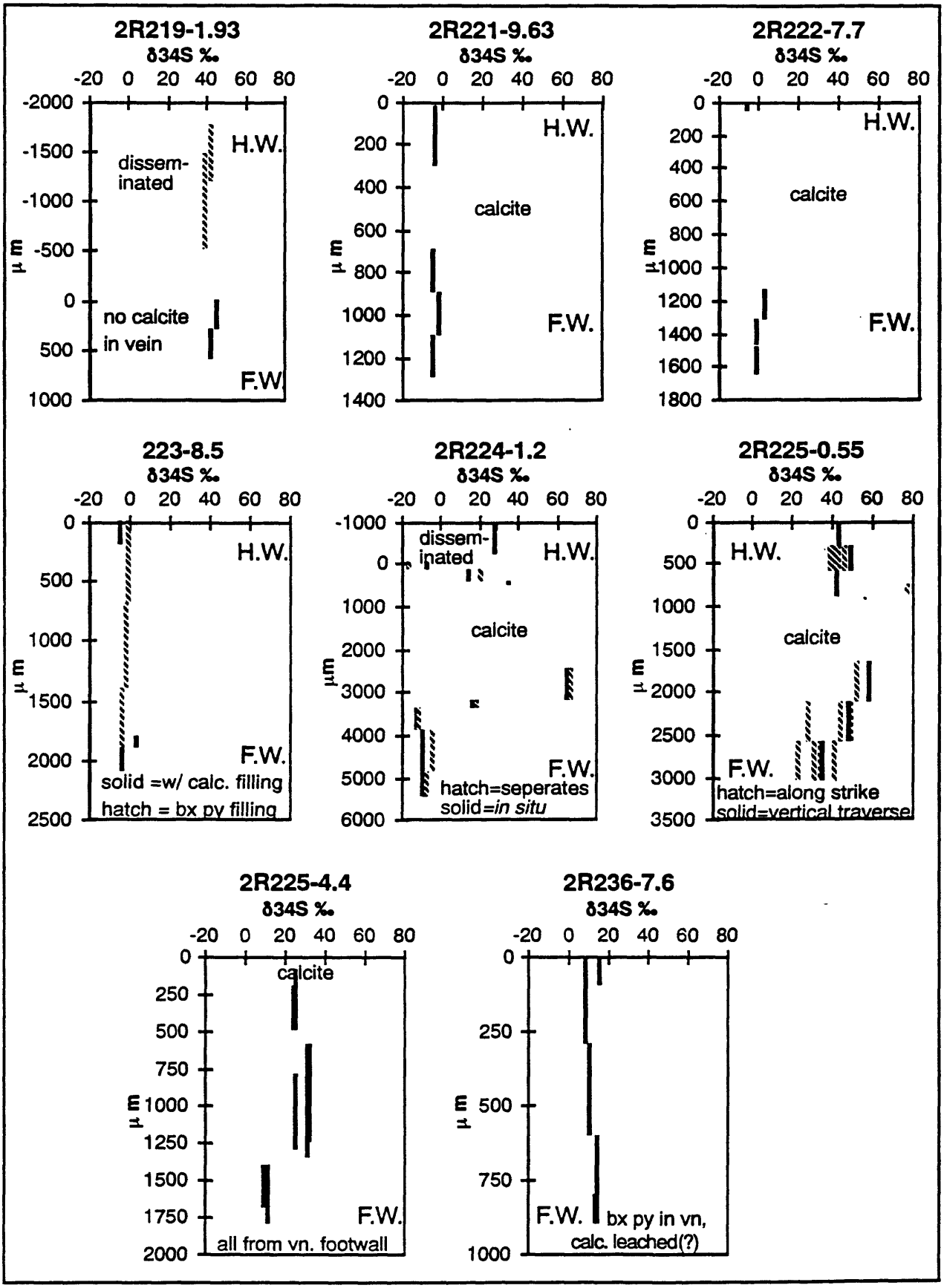
2R219-1.93
δ34S ‰
-20 0 20 40 60 80
-2000
-1500
-1000
-500
0
500
1000
µm
dissem-
inated
H.W.
no calcite
in vein
F.W
2R221-9.63
δ34S ‰
-20 0 20 40 60 80
0
200
400
600
800
1000
1200
1400
µm
H.W.
calcite
F.W.
2R222-7.7
δ34S ‰
-20 0 20 40 60 80
0
200
400
600
800
1000
1200
1400
1600
1800
µm
H.W.
calcite
F.W.
223-8.5
δ34S ‰
-20 0 20 40 60 80
0
500
1000
1500
2000
2500
µm
H.W.
F.W.
solid =w/ calc. filling
hatch = bx py filling
2R224-1.2
δ34S ‰
-20 0 20 40 60 80
-1000
0
1000
2000
3000
4000
5000
6000
µm
dissem-
inated
H.W.
calcite
F.W.
hatch=seperates
solid=in situ
2R225-0.55
δ34S ‰
-20 0 20 40 60 80
0
500
1000
1500
2000
2500
3000
3500
µm
H.W.
calcite
F.W.
hatch=along strike
solid=vertical traverse
2R225-4.4
δ34S ‰
-20 0 20 40 60 80
0
250
500
750
1000
1250
1500
1750
2000
µm
calcite
F.W.
all from vn. footwall
2R236-7.6
δ34S ‰
-20 0 20 40 60 80
0
250
500
750
1000
µm
F.W.
bx py in vn,
calc. leached(?)

Fig. 3.

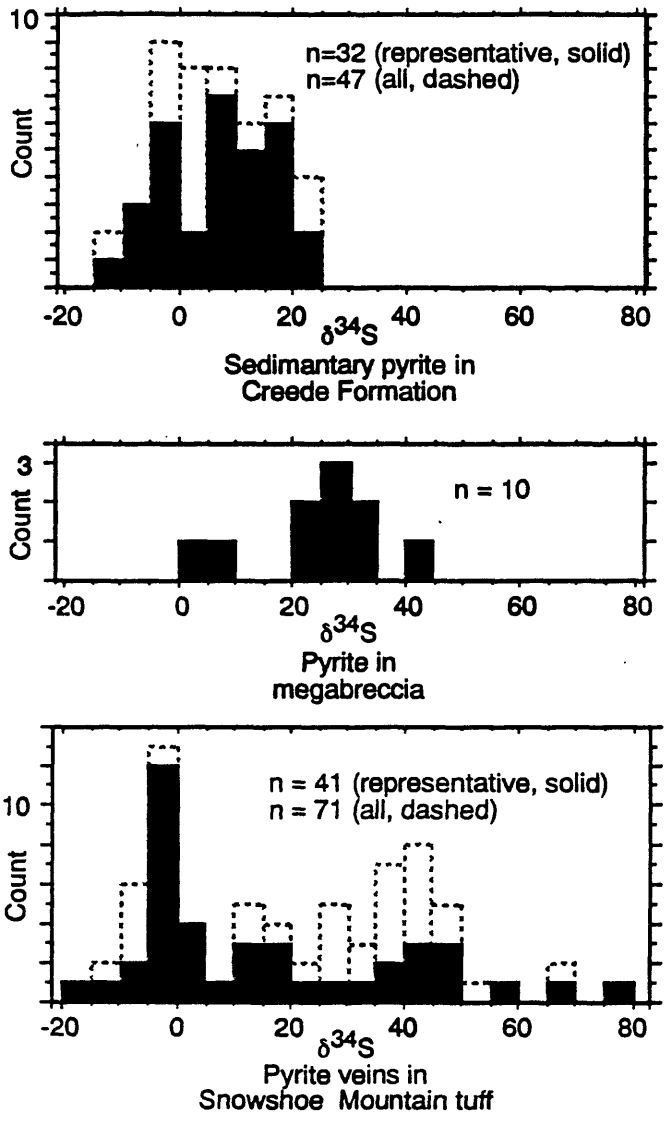
10
Count
n=32 (representative, solid)
n=47 (all, dashed)
-20
0
20
40
60
80
δ34S
Sedimantary pyrite in
Creede Formation
3
Count
n = 10
-20
0
20
40
60
80
δ34S
Pyrite in
megabreccia
10
Count
n = 41 (representative, solid)
n = 71 (all, dashed)
-20
0
20
40
60
80
δ34S
Pyrite veins in
Snowshoe Mountain tuff

Fig. 4.

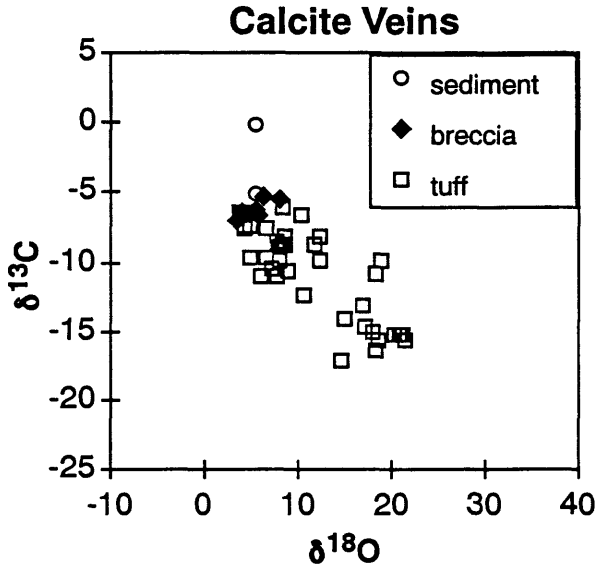
Calcite Veins
sediment
breccia
tuff
5
0
-5
-10
-15
-20
-25
δ13C
-10
0
10
20
30
40
δ18O

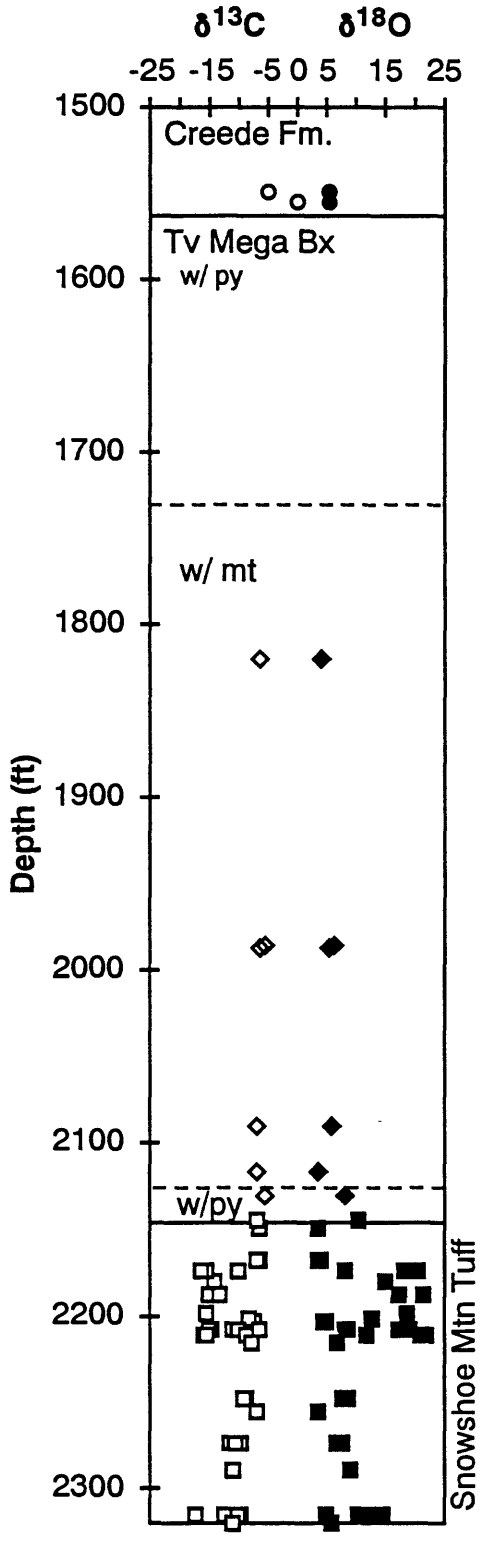
δ13C δ18O
-25 -15 -5 0 5 15 25
1500
Creede Fm.
Tv Mega Bx
w/ py
1600
1700
w/ mt
1800
1900
2000
2100
w/py
2200
2300
Depth (ft)
Snowshoe Mtn Tuff

Fig. 5.

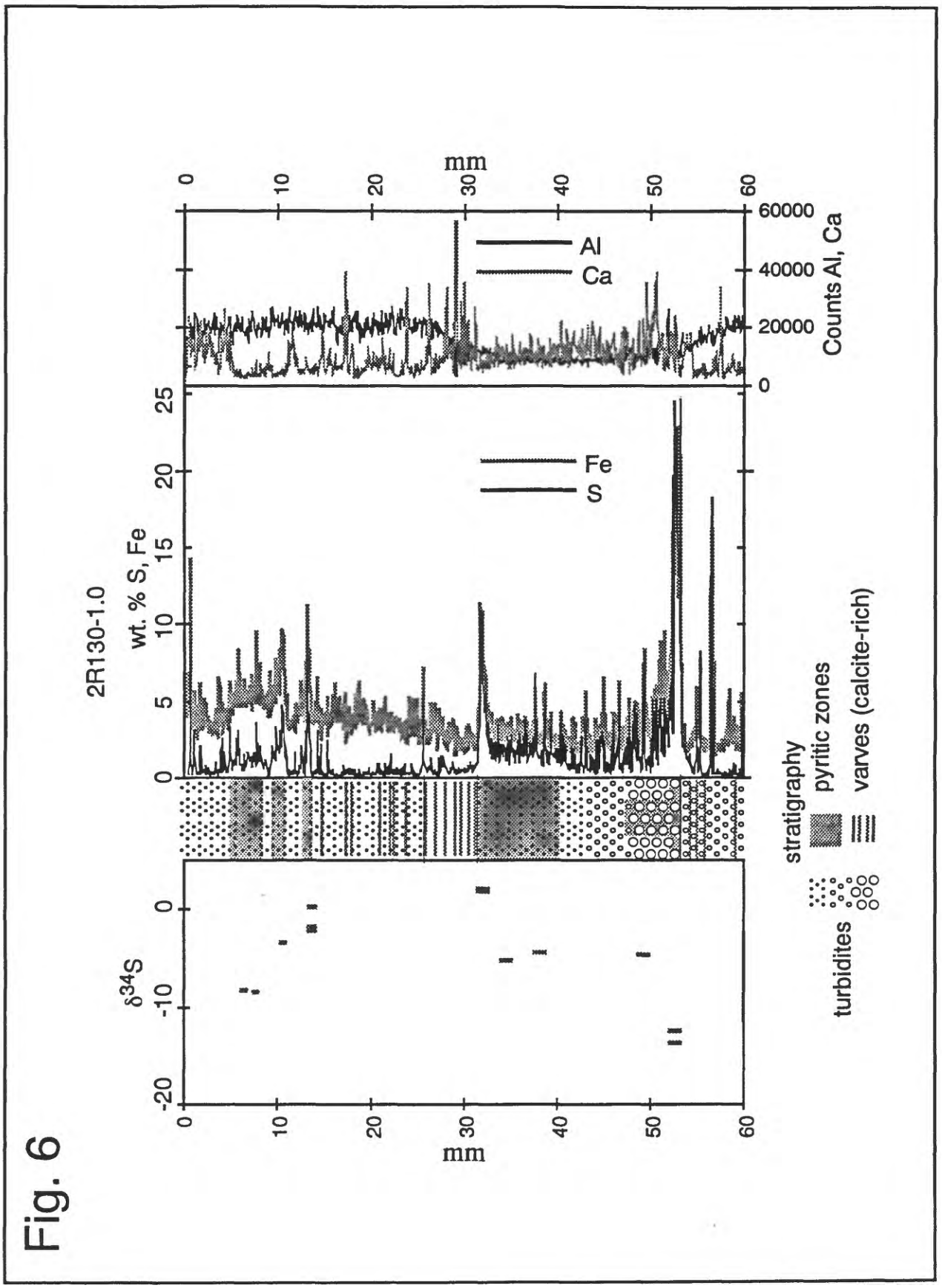
2R130-1.0
wt. % S, Fe
Al
Ca
Counts Al, Ca
Fe
S
mm
δ34S
stratigraphy
pyritic zones
varves (calcite-rich)
turbidites

Fig. 6

Fig. 7.

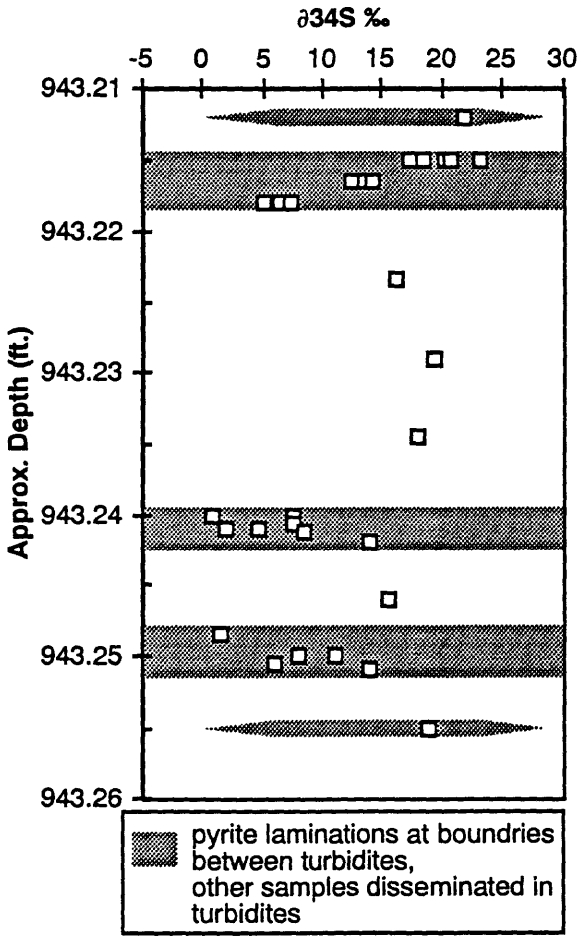
∂34S ‰
-5
0
5
10
15
20
25
30
943.21
943.22
943.23
943.24
943.25
943.26
Approx. Depth (ft.)
pyrite laminations at boundries between turbidites,
other samples disseminated in turbidites

Fig. 8.

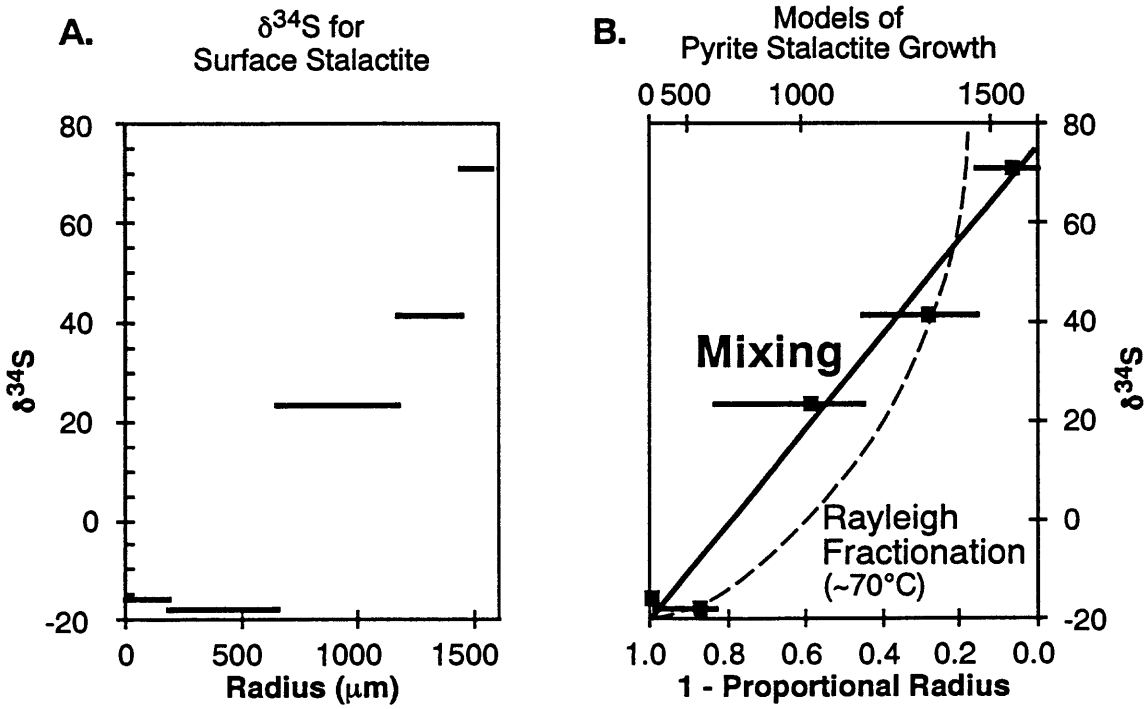
A.
δ34S for
Surface Stalactite
80
60
40
20
0
-20
δ34S
0
500
1000
1500
Radius (μm)
B.
Models of
Pyrite Stalactite Growth
0 500
1000
1500
Mixing
Rayleigh
Fractionation
(~70°C)
1.0
0.8
0.6
0.4
0.2
0.0
1 - Proportional Radius

Fig. 9

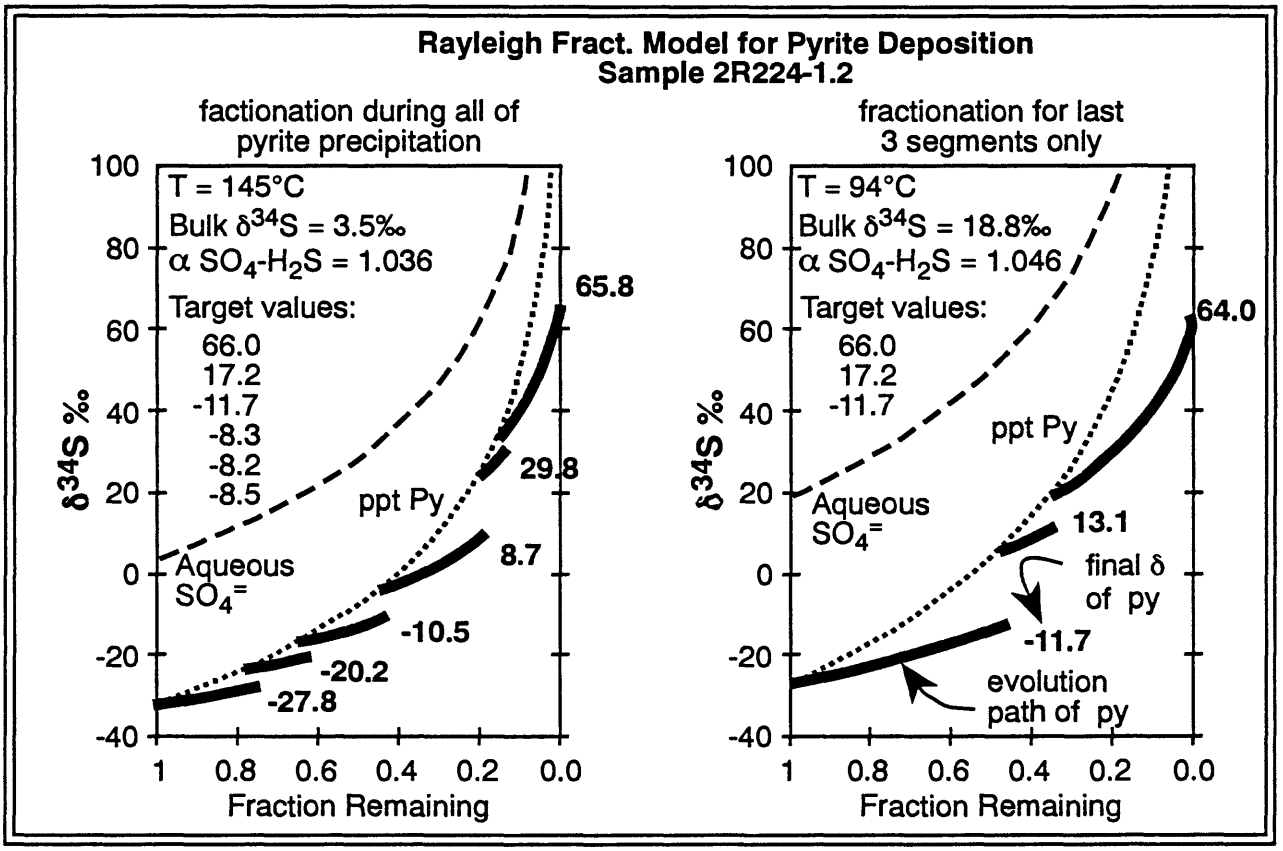
Rayleigh Fract. Model for Pyrite Deposition
Sample 2R224-1.2
factionation during all of pyrite precipitation
T = 145°C
Bulk δ34S = 3.5‰
α SO4-H2S = 1.036
Target values:
66.0
17.2
-11.7
-8.3
-8.2
-8.5
ppt Py
Aqueous SO4=
65.8
29.8
8.7
-10.5
-20.2
-27.8
δ34S ‰
Fraction Remaining
fractionation for last 3 segments only
T = 94°C
Bulk δ34S = 18.8‰
α SO4-H2S = 1.046
Target values:
66.0
17.2
-11.7
ppt Py
Aqueous SO4=
64.0
13.1
final δ of py
-11.7
evolution path of py
δ34S ‰
Fraction Remaining

Early

Fig. 10

Fumaroles release H_2S directly into shallow lake (geysers?)

Pyrite precipitates – when volcanic gases mix with FeOx/silicates during ascent (light S);
– in near-surface regions of hot springs after oxidation/reduction (heavy & light S)

Early lake waters might permeate volcanic substrate

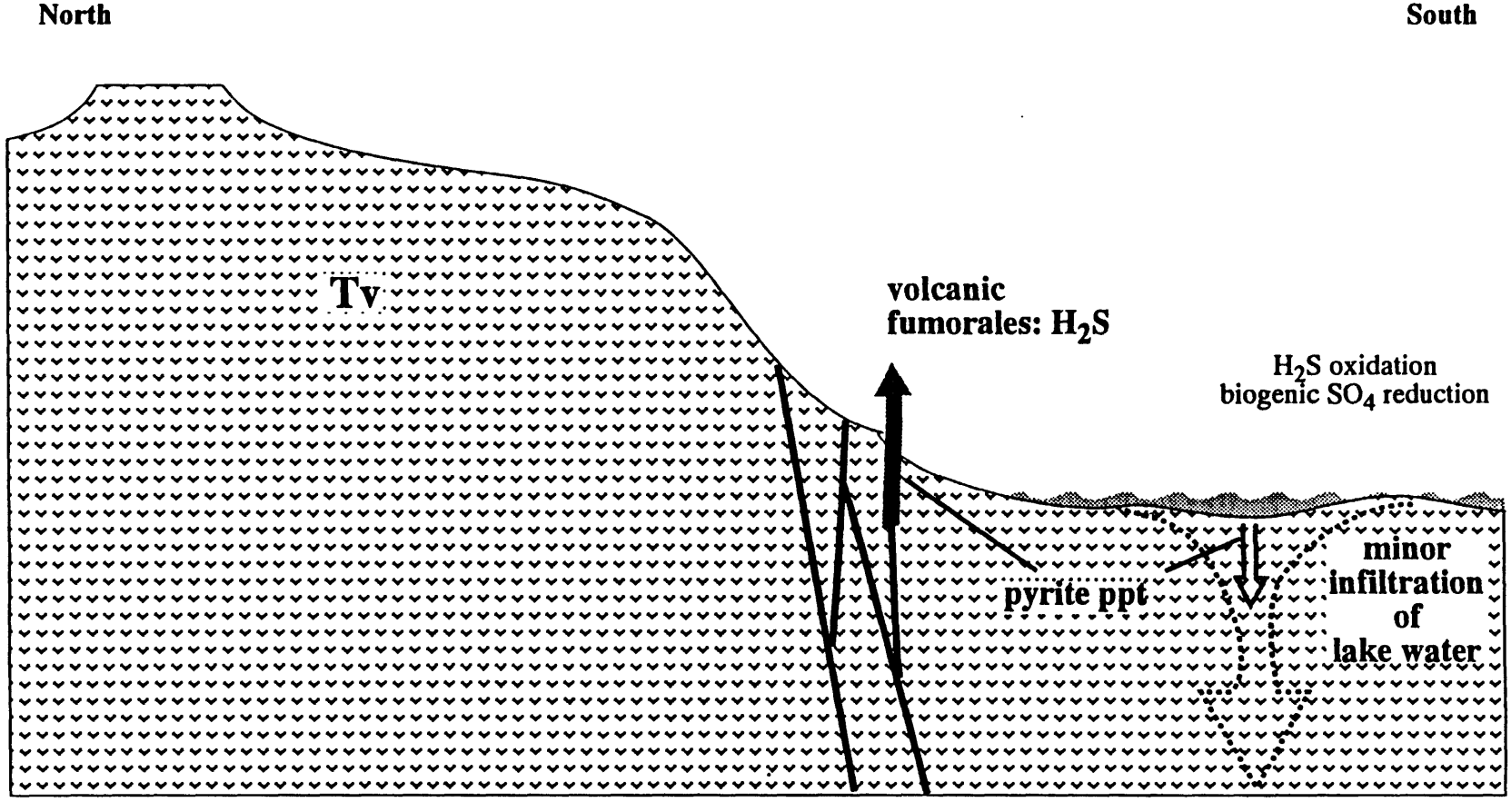

Late

Fig. 11

Minor surface transport of SO_4^{2-} to lake (weathered sulfide?)

Fumaroles release H_2S directly into lake; initiate turbidites

Pyrite precipitation – when FeOx in sediment mixes with H_2S-bearing H_2O
– local bacterial reduction

Little if any water permeates volcanic substrate